Society of Medical Education & Research

2023, Volume 3, Issue 2, Page No: 164-185
ISSN: 3108-4834

Archive of International Journal of Cancer and Allied Science

Synergistic Antitumor Effects of Intratumoral Alum-Anchored IL-12 with Chemotherapy and Immune Checkpoint Inhibition in Syngeneic HNSCC Models

Wei Zhang[1]*, Li Ming[1], Dong Fang[2]

[1]Department of Hematology-Oncology, West China Hospital, Sichuan University, Chengdu, China.
[2] Department of Pathology, Sun Yat-sen University Cancer Center, Guangzhou, China.

***E-mail** ✉ w.zhang.whc@gmail.com

Abstract

The combination of pembrolizumab and chemotherapy is currently used as first-line therapy for recurrent or metastatic head and neck squamous cell carcinoma (HNSCC) and has demonstrated survival benefit. Despite this advance, the proportion of patients who achieve clinical responses with this standard-of-care (SOC) regimen remains relatively low. Interleukin (IL)-12 is a highly active immunostimulatory cytokine that bridges innate and adaptive immune responses and is essential for effective tumor control. Alum-bound murine IL-12 (mANK-101) has previously shown strong antitumor efficacy in multiple syngeneic tumor systems, accompanied by heightened immune activation and extended local cytokine persistence. This work examines the therapeutic potential of adding mANK-101 to SOC therapy in the MOC1 and MOC2 mouse models of HNSCC.C57BL/6 mice implanted with MOC1 or MOC2 tumors received a single intratumoral administration of mANK-101 in combination with weekly intraperitoneal doses of cisplatin and α-programmed death 1 (PD-1) for a total duration of 3 weeks. Immune responses in the MOC1 model were evaluated using flow cytometry and cytokine profiling assays. Multiplex immunofluorescence analysis was conducted to investigate treatment-induced alterations in tumor immune organization. Gene expression analyses were performed to enable detailed characterization of macrophage subsets and effector immune cell populations. Treatment with the triple combination of mANK-101, cisplatin, and α-PD-1 produced the most pronounced suppression of tumor progression and the greatest frequency of tumor-free survival in both MOC1 and MOC2 models, outperforming either mANK-101 alone or SOC therapy with cisplatin plus α-PD-1. This regimen also conferred resistance to tumor re-establishment following rechallenge and limited the growth of non-injected distal tumors. Enhanced antitumor efficacy was associated with increased infiltration of CD8+ T cells, augmented functional activity of both CD8+ and CD4+ T cells, and reprogramming of tumor-associated macrophages from an M2-dominant to an M1-dominant phenotype. Sustained elevation of interferon-γ levels was identified as a central contributor to the observed antitumor effects. Additionally, mice treated with mANK-101 in combination with cisplatin and α-PD-1 developed tertiary lymphoid structure–like immune assemblies in the peritumoral microenvironment. These findings support the use of alum-anchored IL-12 in combination with cisplatin and α-PD-1 as a promising therapeutic strategy for HNSCC.

Keywords: Cytokine, Chemotherapy, Abscopal, Head and neck cancer, Solid tumor

Introduction

Head and neck malignancies constitute the sixth leading cancer type globally, with approximately 890,000 newly diagnosed cases each year at present and forecasts estimating an increase to nearly 1.08 million new cases annually by 2030 [1, 2]. Roughly 90% of these tumors arise from the mucosal lining of the oral cavity, pharynx, and larynx and are collectively classified as head and neck squamous cell carcinoma (HNSCC) [3]. Established risk factors for HNSCC include prior infection with oncogenic human papillomavirus (HPV) strains, exposure to tobacco-related carcinogens, alcohol intake, and betel nut chewing [1, 3]. For patients with recurrent or metastatic (R/M) HNSCC, the current standard-of-

Access this article online https://smerpub.com/

Received: 21 May 2023; **Accepted:** 29 October 2023

How to cite this article: Zhang W, Ming L, Fang D. Synergistic Antitumor Effects of Intratumoral Alum-Anchored IL-12 with Chemotherapy and Immune Checkpoint Inhibition in Syngeneic HNSCC Models. Arch Int J Cancer Allied Sci. 2023;3(2):164-85. https://doi.org/10.51847/0qciKhjaqh

care (SOC) consists of the programmed death 1 (PD-1) inhibitor pembrolizumab, administered either alone or together with platinum-based chemotherapy and 5-fluorouracil (5-FU) [4, 5]. While this regimen has produced durable clinical benefit, objective responses are observed in only about one-third of patients, underscoring the need to further optimize SOC approaches for HNSCC.

Interleukin-12 (IL-12) is a multifunctional proinflammatory cytokine secreted by antigen-presenting cells (APCs) that coordinates interactions between innate and adaptive immune responses. IL-12 enhances cytotoxic functions of CD8+ T cells, natural killer (NK) cells, and natural killer T (NKT) cells, while also promoting T helper 1 (Th1) differentiation [6]. Despite its strong immunostimulatory capacity, clinical development of IL-12 therapies has been limited by insufficient efficacy and dose-limiting toxicities associated with systemic exposure [7]. Consequently, approaches that prolong IL-12 activity while restricting systemic toxicity are critically needed. Several tumor-localized delivery strategies—such as intratumoral (i.t.) administration of IL-12–encoding plasmids or messenger RNA, as well as subcutaneous injection of IL-12–based immunocytokines—have demonstrated antitumor activity in preclinical models [8] and acceptable safety profiles in multiple phase I clinical trials [9–13]. Given its accessibility and tendency toward local recurrence, HNSCC represents a suitable indication for i.t. delivery of emerging therapeutic agents [14], including alum-tethered IL-12 formulations.

More recently, a novel alum-anchored IL-12 platform has been developed to enable safe and effective cytokine delivery [15, 16]. This construct consists of recombinant IL-12 fused to an aluminum-binding peptide (ABP) and co-expressed with a single kinase (Fam20C), which mediates site-specific phosphorylation of serine residues within the ABP. Following phosphorylation, the ABP exhibits strong affinity for hydroxyl groups on the US Food and Drug Administration–approved vaccine adjuvant aluminum hydroxide (Alhydrogel), resulting in a stable complex. Upon i.t. injection, the IL-12–ABP/Alhydrogel formulation, termed ANK-101, forms a localized depot that prolongs intratumoral cytokine retention and mitigates the rapid clearance typically observed with i.t. cytokine delivery [15, 16]. The murine analog of ANK-101, designated mANK-101, has demonstrated antitumor activity in both immunologically "hot" (MC38, CT26) and "cold" (4T1, B16F10) syngeneic tumor models [15, 16]. Prior studies have also shown that mANK-101 can act synergistically with immune checkpoint inhibitors to enhance tumor-free survival. Mechanistically, mANK-101 treatment increased effector cell infiltration, amplified proinflammatory signaling, and reshaped the tumor microenvironment (TME) [15, 16].

In the present work, we report for the first time the antitumor activity of mANK-101 combined with cisplatin and α-PD-1 in HPV-negative MOC1 and MOC2 murine head and neck cancer models. Relative to mANK-101 alone or SOC therapy consisting of cisplatin plus α-PD-1, the combination regimen produced stronger tumor control and extended survival. The observed antitumor effects were closely linked to enhanced CD8+ T-cell infiltration and cytotoxic function, increased CD4+ T-cell activity, maturation of NK cells, and a shift in tumor-associated macrophages from an M2 to an M1 phenotype within the tumor microenvironment. Interferon (IFN)-γ emerged as a central mediator of the immune response induced by the combination therapy. Moreover, treatment with mANK-101+cisplatin+α-PD-1 promoted the development of tertiary lymphoid structure (TLS)-like immune aggregates in the MOC1 model. Collectively, these findings establish a preclinical rationale for incorporating mANK-101 into first-line SOC regimens for locoregionally relapsed HNSCC to determine whether patient response rates and overall benefit can be improved.

Materials and Methods

Cell lines, animals, and reagents

Parental stocks of MOC1 and MOC2 cell lines were obtained from R. Uppaluri at Washington University (St. Louis, Missouri, USA) and maintained under previously reported culture conditions [17]. All cell lines were used at low passage numbers (<20) and confirmed to be free of Mycoplasma contamination. Wild-type C57BL/6 mice were bred and housed at the National Institutes of Health (Bethesda, Maryland, USA) in pathogen-free microisolator facilities.

Murine IL-12–ABP (mIL-12-ABP), as described previously [15], was supplied through a Cooperative Research and Development Agreement between Ankyra Therapeutics (Cambridge, Massachusetts, USA) and the National Cancer Institute (Bethesda, Maryland, USA). The mANK-101 formulation was generated by combining 0.25 mg/mL mIL-12-ABP with 2.5 mg/mL

Alhydrogel (InvivoGen, San Diego, California, USA) in Tris-buffered saline (TBS) and incubating the mixture for 30 min at room temperature. Prepared complexes were administered within 4 hours of formulation.

In vivo experiments

All animal experiments were performed under approval of the NIH Institutional Animal Care and Use Committee (protocol CIO-2) and adhered to ARRIVE reporting standards [18]. On day 0, female C57BL/6 mice (8–12 weeks of age) were subcutaneously (s.c.) inoculated in the right flank with either 5×10^6 MOC1 cells or 1×10^5 MOC2 cells combined at a 1:1 ratio with Matrigel. For bilateral tumor studies, s.c. injections were administered to both right and left flanks on the same day. In the majority of experiments, mice received a single intratumoral (i.t.) injection of mANK-101 (5 µg in 20 µL) on day 10, corresponding to a mean tumor volume of 120–200 mm^3. Cisplatin was administered intraperitoneally (i.p.) at 5 mg/kg (West-Ward Pharmaceuticals, Eatontown, New Jersey, USA), together with 200 µg α-PD-1 antibody (Clone RMP1-14; Bio X Cell, Lebanon, New Hampshire, USA), on days 10, 17, and 24.

For immune depletion experiments, mice were treated i.p. with 100 µg α-CD4 (Clone GK1.5), 100 µg α-CD8 (Clone 2.43), or 100 µg α-NK1.1 (Clone PK136) antibodies on days 6, 7, and 8, followed by weekly dosing thereafter. Neutralization studies involved i.p. administration of 100 µg α-IFN-γ (Clone XMG1.2) or 300 µg α-CSFR1 (Clone AFS98) on days −2, 0, and +2 relative to each treatment cycle, followed by dosing three times per week. All depletion and neutralization antibodies were sourced from Bio X Cell (Lebanon, New Hampshire, USA). Tumor volumes were calculated using the formula length×$width^2$/2. Animals were euthanized upon reaching predefined endpoints, including tumor length of 20 mm, tumor volume exceeding 2,000 mm^3, ulceration affecting 50% of the tumor surface, or body weight loss greater than 20%.

Flow cytometry

Tumors were excised and processed through combined mechanical dissociation and enzymatic digestion to obtain single-cell suspensions. Prior to antibody staining, Fc receptors were blocked using anti-CD16/32 antibodies (Clone 2.4G2; BD Biosciences, Franklin Lakes, New Jersey, USA). Cells were then stained with fluorophore-conjugated antibodies. BioLegend (San Diego, California, USA) antibodies included CD44-BV421 (IM7), CD4-BV605 (RM4-5), IFNγ-BV785 (XMG1.2), granzyme B-FITC (GB-11), CD38-BV421 (90), F4/80-BV605 (BM8), and CD206-PECy7 (C06802). Antibodies obtained from BD Biosciences included CD62L-BV711 (MEL-14), CD8-PerCP-Cy5.5 (53–6.7), CD3-APC-Cy7 (17A2), CD11b-PerCP-Cy5.5 (M1/70), CD49b-PE (DX5), CD27-PECy7 (LG3A10), CD11c-FITC (HL3), and CD19-APC (ID3). Invitrogen (Waltham, Massachusetts, USA) reagents included CD45-BUV737 (30-F11), FoxP3-PE (FJK-16s), and Ki67-PECy7 (SolA15).

Antigen-specific CD8+ T cells were identified using H-2Kb MuLV p15E Tetramer-KSPWFTTL-APC together with CD8-PE (Clone KT15), both from MBL International Corporation (Woburn, Massachusetts, USA). Intracellular staining was conducted using the FoxP3/transcription factor staining kit (eBioscience, San Diego, California, USA) according to manufacturer instructions. Nonviable cells were excluded using a fixable live/dead blue viability dye (Thermo Fisher, Waltham, Massachusetts, USA). Data acquisition was performed on a BD Fortessa cytometer (BD Biosciences) using FACSDiva software, and downstream analysis was completed with FlowJo v10.8.2 (TreeStar, Ashland, Oregon, USA). Gating strategies involved FSC×SSC selection followed by FSC-A×FSC-H discrimination. Immune populations were defined as follows: CD4+ T cells (live/CD45+/CD3+/CD4+/CD8−/FoxP3−), CD8+ T cells (live/CD45+/CD3+/CD4−/CD8+), regulatory T cells (live/CD45+/CD3+/CD4+/CD8−/FoxP3+), NK cells (live/CD45+/CD3−/CD49b+), and macrophages (live/CD45+/CD3−/CD11c−/CD19−/CD11b+/F4/80+).

Multiplex cytokine array

Cytokine profiling of serum and tumor samples was performed using the LEGENDplex Mouse Inflammation Panel (BioLegend, San Diego, California, USA) following the manufacturer's protocol. Serum samples were generated from blood collected via mandibular bleeding. Tumor supernatants were prepared by homogenizing tissue in phosphate-buffered saline using a gentleMACS Dissociator (Miltenyi Biotec, Bergisch Galdbach, Germany).

H&E staining, multiplex immunofluorescence staining, and multispectral imaging

Resected tumors were fixed in formalin and submitted to VitroVivo Biotech (Gaithersburg, Maryland, USA) for

paraffin embedding, sectioning, and hematoxylin and eosin (H&E) staining. Multiplex immunofluorescence was carried out using Opal 6-Plex Tyramine Signal Amplification kits according to manufacturer guidelines (Akoya Biosciences, Marlborough, Massachusetts, USA). The staining panel consisted of DAPI, CD11c, CD103, CXCL13, B220, CD19, and CD8. Slide preparation steps, including deparaffinization, rehydration, antigen retrieval, and staining, were automated using the BOND RX Autostainer (Leica, Nussloch, Germany). Optimal staining conditions were established through single-marker immunohistochemistry and immunofluorescence prior to multiplex application. Whole-slide imaging was performed using the PenoImager HT scanner (Akoya Biosciences) at 20× magnification.

Immune aggregate quantification

Immune aggregates were manually counted across entire tumor sections based on multiplex immunofluorescence staining. Aggregates were defined by compact clustering of B220+CD19+ B cells, CD8+ T cells, and CD11c+ dendritic cells expressing CXCL13 and CD103. Regions containing immune markers without clear cellular colocalization were excluded from analysis. Aggregate identification was validated using corresponding H&E-stained sections.

RNA analysis

Tumors were processed via mechanical disruption and enzymatic digestion to generate single-cell suspensions. For each treatment group, equal numbers of viable cells from individual tumors were pooled. CD45+ immune cells were isolated using the Mouse CD45 Isolation Kit (Miltenyi Biotec, Bergisch Galdbach, Germany) following manufacturer instructions. Total RNA was extracted using the RNeasy Mini Kit (Qiagen, Hilden, Germany). Gene expression profiling was conducted using the nCounter PanCancer Immune Profiling Panel and the nCounter Mouse Myeloid Innate Immunity Gene Expression Panel (NanoString Technologies, Seattle, Washington, USA) at the Genomics Laboratory, Frederick National Laboratory for Cancer Research. Data normalization and analysis were performed with nSolver software v4.0.70 (NanoString Technologies), using housekeeping genes for normalization and untreated samples as categorical references. Pathway analysis was carried out with Ingenuity Pathway Analysis (Qiagen), applying fold-change thresholds of −1.5 and 1.5. Relative immune cell abundance was estimated using ROSALIND with the NanoString Cell Type Profiling Module.

Statistical analysis

Comparisons involving more than two groups were performed using one-way or two-way analysis of variance, followed by Tukey's multiple-comparisons test for adjustment. Survival distributions were evaluated using the log-rank (Mantel–Cox) test. Fisher's exact test was employed for pathway-level analyses. Statistical significance was defined as $P < 0.05$. Data are presented as mean ± SEM. All statistical analyses and graphical outputs were generated using GraphPad Prism version 10.2.3.

Results and Discussion

Combination treatment with mANK-101, cisplatin, and α-PD-1 produces antitumor activity in MOC1 and MOC2 murine oral squamous cell carcinoma models

Pembrolizumab (α-PD-1) administered with platinum-based chemotherapy (cisplatin or carboplatin) plus fluorouracil currently represents the recommended first-line therapy for recurrent or metastatic HNSCC [4, 5]. To model this standard-of-care (SOC) regimen in mice, MOC1 tumor–bearing animals were treated with weekly doses of α-PD-1 combined with cisplatin and 5-FU. Because clinical data from locally advanced HNSCC indicate that patients receiving carboplatin plus 5-FU complete chemotherapy less frequently than those receiving cisplatin due to toxicity [19], the efficacy of α-PD-1 combined with cisplatin alone was also evaluated. Both cisplatin+α-PD-1 ($p = 0.0105$) and 5-FU+cisplatin+α-PD-1 ($p = 0.0426$) induced statistically significant but limited tumor growth suppression in the MOC1 model (**Figure 1a**), without detectable treatment-related toxicity**.** Based on these findings, cisplatin combined with α-PD-1 was selected as the SOC comparator for subsequent experiments.

mANK-101 consists of a single-chain murine IL-12 molecule containing both p40 and p35 subunits, fused to a C-terminal phosphorylated aluminum-binding peptide (ABP) and complexed with Alhydrogel [15, 16]. Prior work demonstrated that intratumoral delivery of mANK-101 leads to antitumor responses across multiple syngeneic tumor models, coinciding with prolonged intratumoral retention of the IL-12 complex. Consistent with these reports, mANK-101 monotherapy suppressed

tumor growth in MC38 tumors of varying genotypes, although efficacy declined as tumor size increased at the time of treatment **(Figure 2).**

To assess whether mANK-101 could enhance SOC efficacy in MOC1 tumors, a single intratumoral dose of mANK-101 was combined with weekly systemic administration of cisplatin and α-PD-1 **(Figure 1a).** Treatment with cisplatin+α-PD-1 alone delayed tumor progression ($p < 0.0001$; **Figure 1b**) and extended survival ($p = 0.0013$; **Figure 1d**) relative to untreated controls but failed to achieve complete tumor regression **(Figure 1c).** In contrast, mANK-101 monotherapy resulted in improved tumor control compared with untreated mice ($p < 0.0001$) and SOC-treated mice ($p = 0.003$; **Figure 1b**), with 2 of 10 animals remaining tumor-free at study completion **(Figure 1c)** and significantly prolonged survival compared with both untreated ($p < 0.0001$) and SOC groups ($p = 0.0094$; **Figure 1d**).

Notably, the combination of mANK-101 with cisplatin and α-PD-1 produced the strongest therapeutic benefit, yielding superior tumor growth inhibition relative to untreated controls ($p < 0.0001$), mANK-101 alone ($p = 0.0194$), and SOC therapy ($p < 0.0001$; **Figure 1b**). This triple-therapy regimen also generated the highest proportion of tumor-free animals (5 of 10; **Figure 1c)** and significantly improved median overall survival compared with untreated mice ($p = 0.0001$), mANK-101 monotherapy ($p = 0.0153$), and cisplatin+α-PD-1 treatment ($p = 0.0002$; **Figure 1d**). When the treatment schedule was modified such that mANK-101 administration occurred 1 week after initiation of cisplatin+α-PD-1, the triple combination remained superior to both mANK-101 alone ($p = 0.009$) and SOC therapy ($p = 0.0138$; **Figure 3**). Moreover, mANK-101 combined with cisplatin and α-PD-1 produced antitumor efficacy and tolerability comparable to regimens that also included 5-FU **(Figures 1c and 1d),** supporting the adequacy of cisplatin+α-PD-1 as SOC in the MOC1 model.

Importantly, mice rendered tumor-free by mANK-101+cisplatin+α-PD-1 therapy exhibited durable protection against tumor relapse, with 66.6% of animals resisting tumor regrowth following rechallenge with 5×10^6 MOC1 cells **(Figure 1e).** Prior exposure to the combination therapy also significantly extended survival after rechallenge compared with tumor-naïve mice ($p = 0.0005$; **Figure 1f**).

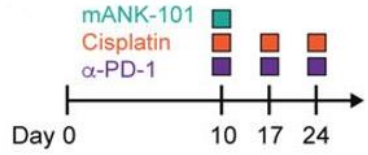

a)

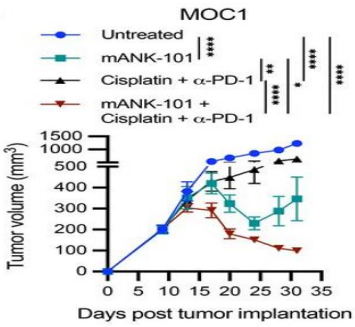

b)

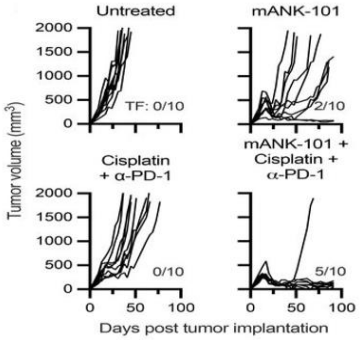

c)

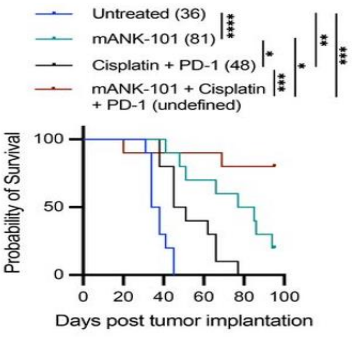

d)

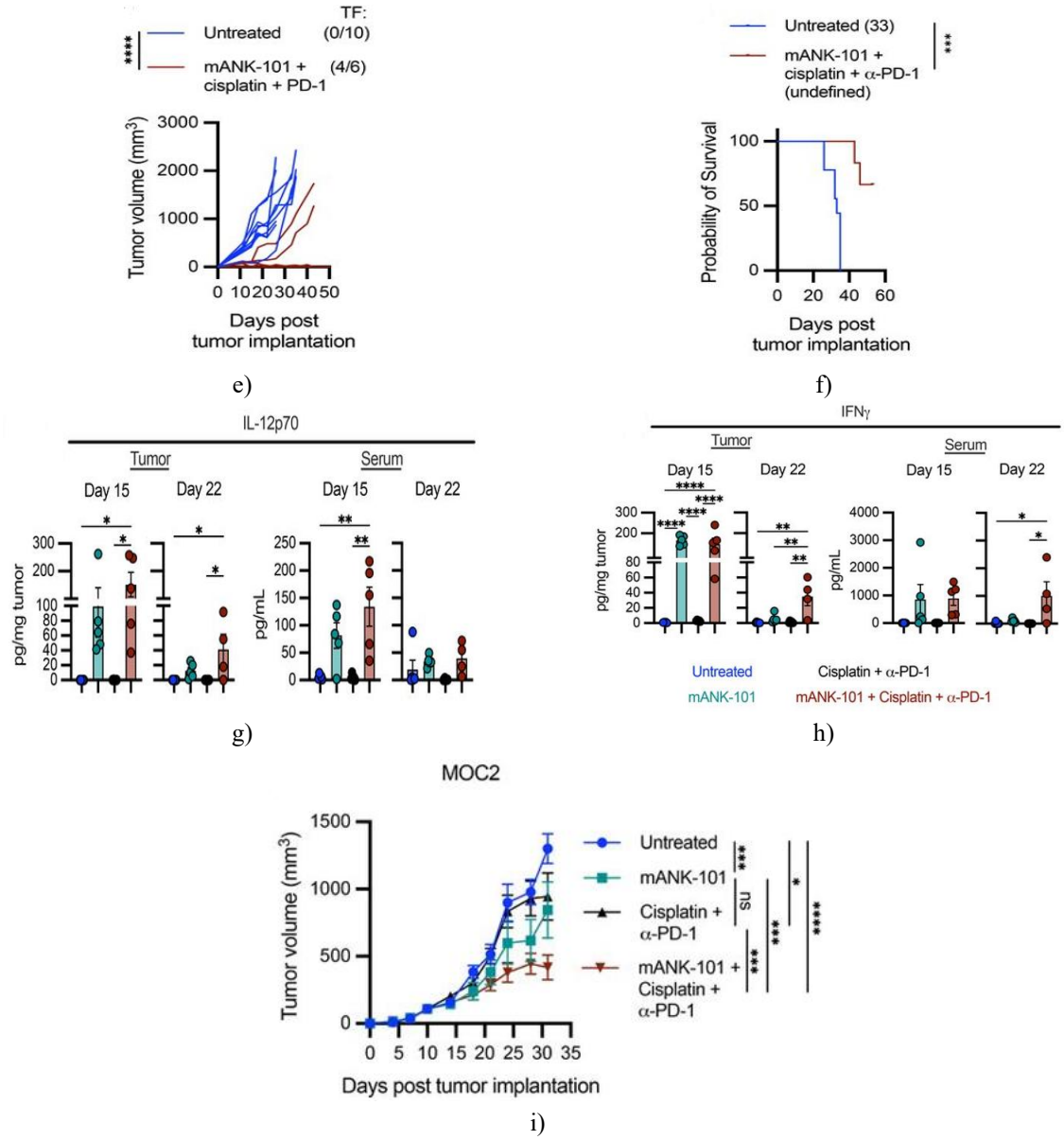

Figure 1. Antitumor activity of combined mANK-101, cisplatin, and α-PD-1 treatment in murine MOC1 and MOC2 oral squamous cell carcinoma models.

(a–d) Female C57BL/6 mice aged 8–12 weeks (n=10 per treatment arm) were subcutaneously inoculated in the right flank with 5×10^6 MOC1 cells on day 0. When tumors reached an average size of approximately 200 mm^3, a single intratumoral (i.t.) dose of mANK-101 (5 µg) was administered on day 10. Concurrently, mice received intraperitoneal (i.p.) injections of cisplatin (5 mg/kg) and α-PD-1 antibody (200 µg) on days 10, 17, and 24, as depicted in the treatment scheme (a). Tumor dimensions were measured longitudinally. (b) Group-averaged tumor growth kinetics and (c) individual tumor trajectories are shown. Insets indicate the number of mice achieving a tumor-free (TF) outcome at study termination. (d) Overall survival was monitored, with values in parentheses indicating median overall survival (mOS).

(e–f) An independent cohort of MOC1 tumor–bearing mice was treated using the same regimen described in (a). On day 55, animals that remained tumor-free following triple therapy were rechallenged with 5×10^6 MOC1 cells. Age-matched naïve C57BL/6 mice served as untreated

controls. (e) Mean tumor growth following rechallenge and (f) post-rechallenge survival were evaluated.

(g–h) Female C57BL/6 mice (8–12 weeks old; n=8 per group) were implanted bilaterally with 5×10^6 MOC1 cells per flank and treated as outlined in (a). Serum and primary tumor samples (n=4–5 per group) were collected on days 15 and 22 and subjected to multiplex cytokine profiling. Concentrations of (g) IL-12p70 and (H) IFN-γ are shown.

(i) Female C57BL/6 mice (8–12 weeks old; n=8 per group) bearing 1×10^5 MOC2 tumors were treated according to the same protocol described in (a). Tumor burden was monitored over time, and mean tumor volumes are presented.

Statistical analyses included two-way ANOVA with Tukey's post hoc correction for tumor growth, Mantel–Cox testing for survival comparisons, and one-way ANOVA with Tukey's correction for intergroup analyses. Error bars indicate SEM. *p<0.05, **p<0.01, ***p<0.001, ****p<0.0001. Abbreviations: ANOVA, analysis of variance; IFN, interferon; i.p., intraperitoneal; mOS, median overall survival; ns, not significant; PD-1, programmed death 1; TF, tumor-free.

Cytokine profiling demonstrated that the therapeutic benefit associated with mANK-101+cisplatin+α-PD-1 coincided with enhanced inflammatory cytokine accumulation within the tumor microenvironment **(Figures 1g,h).** Intratumoral IL-12 levels were significantly increased in the triple-therapy group at day 15 (p=0.0134) and remained elevated at day 22 (p=0.0248; **Figure 1g).** In contrast, circulating IL-12 showed a transient increase at day 15 (p=0.0134) before returning to baseline by day 22 **(Figure 1g).** Both mANK-101 alone (p<0.0001) and mANK-101+cisplatin+α-PD-1 (p<0.0001) induced robust IFN-γ production in tumors at day 15 relative to untreated controls **(Figure 1h)**. By day 22, IFN-γ levels normalized in tumors receiving mANK-101 monotherapy, whereas sustained elevation persisted exclusively in the triple-combination group (p=0.0018; **Figure 1h**). Although serum IFN-γ increased by approximately 10-fold at day 15 following both mANK-101 monotherapy and triple therapy, these changes were not statistically significant **(Figure 1h).** Notably, only mice treated with mANK-101+cisplatin+α-PD-1 maintained significantly elevated serum IFN-γ at day 22 (p=0.0368; **Figure 1h**). These data collectively indicate that the triple regimen establishes a prolonged pro-inflammatory state within the tumor.

Because immunologically responsive tumors such as MOC1 demonstrate heightened sensitivity to immunotherapy [20, 21], the efficacy of mANK-101+cisplatin+α-PD-1 was further evaluated in the poorly immunogenic MOC2 model [20]. In this setting, both mANK-101 monotherapy and cisplatin+α-PD-1 produced only partial suppression of tumor growth relative to controls (p=0.003 and p=0.0263, respectively; **Figure 1i).** In contrast, the triple-combination regimen significantly inhibited tumor progression compared with untreated animals (p<0.0001), mANK-101 alone (p=0.0005), and cisplatin+α-PD-1 (p=0.0001). Taken together, these findings demonstrate that mANK-101+cisplatin+α-PD-1 sustains intratumoral IL-12 and IFN-γ signaling and is effective against both immunogenic and therapy-resistant oral squamous cell carcinoma models.

Previous work has established that combining mANK-101 with α-PD-1 enhances antitumor responses in multiple murine tumor systems [15, 16]. To determine whether dual combinations were sufficient in the MOC1 model, mANK-101 was administered together with either cisplatin or α-PD-1. Although mANK-101+cisplatin significantly reduced tumor burden compared with untreated controls (p=0.0006), its efficacy did not exceed that of mANK-101 monotherapy (p=0.8843; **Figure 2a**). Similarly, mANK-101+α-PD-1 produced strong tumor growth inhibition versus control animals (p=0.0004), yet did not differ statistically from mANK-101 alone (p=0.6797; **Figure 2b**). Consistent with the results shown in **Figure 1**, the triple-combination therapy mANK-101+cisplatin+α-PD-1 provided superior tumor control relative to mANK-101 monotherapy (p=0.0393; **Figure 2c**) and generated the highest proportion of tumor-free mice **(Figure 2d).** Notably, mANK-101+α-PD-1 treatment resulted in complete tumor clearance in 4 of 11 animals, indicating that although maximal efficacy was achieved with the triple regimen, meaningful therapeutic benefit may also be obtained with the dual combination. All regimens evaluated were well tolerated, with no evidence of treatment-associated toxicity as assessed by stable body weight **(Figure 2e).**

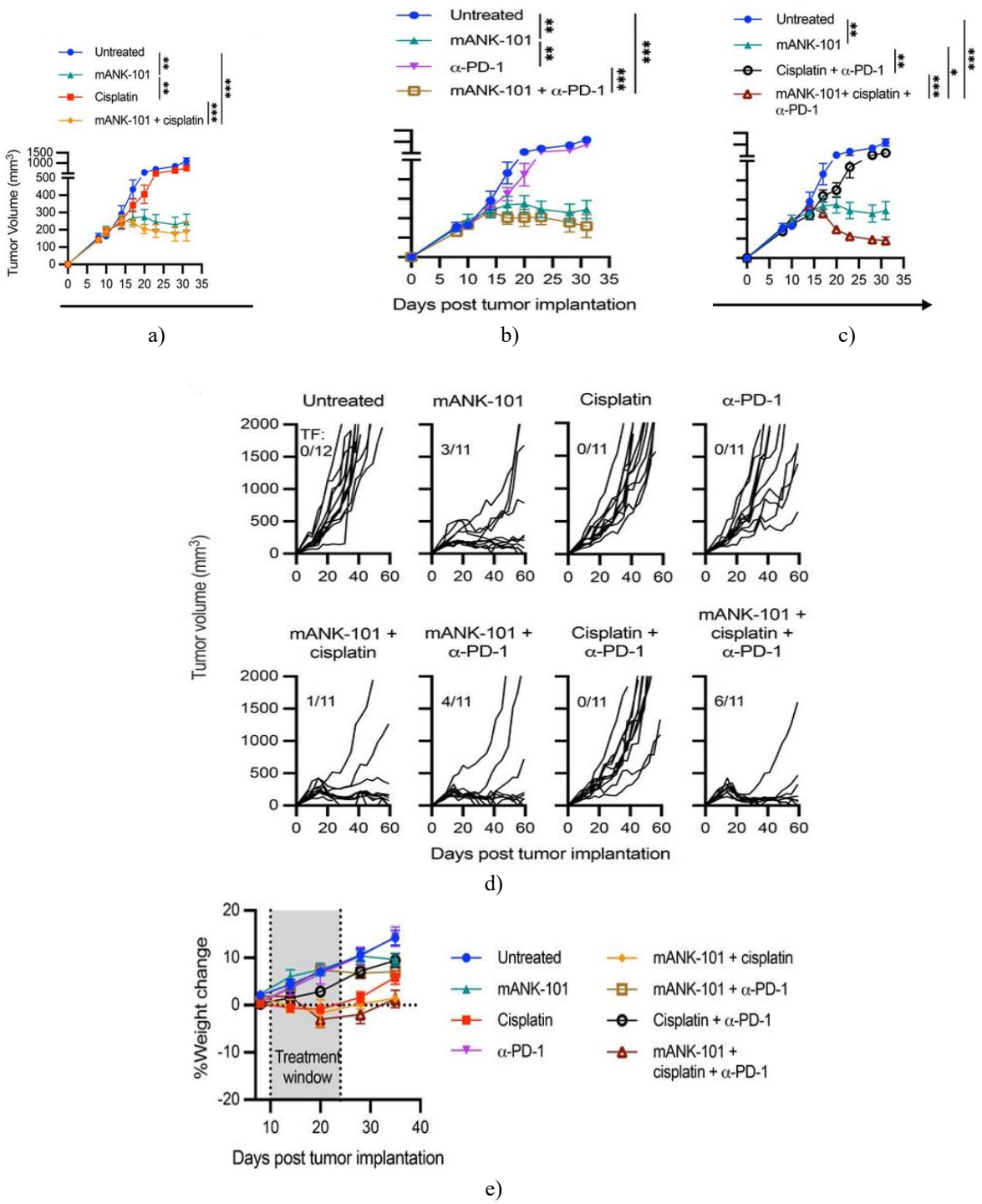

Figure 2. Superior tumor control achieved with mANK-101 combined with cisplatin and α-PD-1 relative to single-agent or two-drug regimens.

Female C57BL/6 mice between 8 and 12 weeks of age (n=11–12 per treatment arm) received subcutaneous implantation of 5×10^6 MOC1 cells into the right flank on day 0. Therapeutic interventions followed the schedule depicted in **Figure 1a**, and animals were observed throughout the study period. (a–c) Average tumor volume trajectories and (d) individual tumor growth profiles are shown. Insets specify the number of animals remaining tumor-free at study termination. (e) Longitudinal body weight measurements were collected

as an indicator of treatment tolerability. Tumor growth comparisons were analyzed using two-way ANOVA with Tukey's multiple comparison correction. Error bars denote SEM. *p<0.05, **p<0.01, ***p<0.001. Abbreviations: ANOVA, analysis of variance; PD-1, programmed death 1; TF, tumor-free.

Triple-combination therapy with mANK-101, cisplatin, and α-PD-1 reshapes antitumor immunity

To investigate treatment-associated immunologic remodeling within tumors, transcriptomic profiling was performed on CD45⁺ leukocytes isolated from tumor tissue 5 days following initiation of therapy, using the NanoString nCounter Mouse PanCancer IO360 Panel. Differential expression analysis demonstrated that both mANK-101 alone and the mANK-101+cisplatin+α-PD-1 regimen markedly elevated transcripts linked to inflammatory signaling, chemotaxis, and immune effector function, with *Ifng* emerging as the most strongly induced gene in both conditions **(Figure 3a).** Consistent with these findings, pathway enrichment analysis identified activation of immune-related signaling modules, including T-cell receptor engagement, IL-12 signaling, IFN-mediated pathways, and antigen processing and presentation, in tumors exposed to mANK-101 monotherapy or the triple-drug combination **(Figure 3b).** Computational cell type inference further revealed an accumulation of cytotoxic T lymphocytes specifically in tumors treated with mANK-101+cisplatin+α-PD-1, accompanied by reduced representation of exhausted T cells and Tregs in both mANK-101–containing treatment groups **(Figure 3c).**

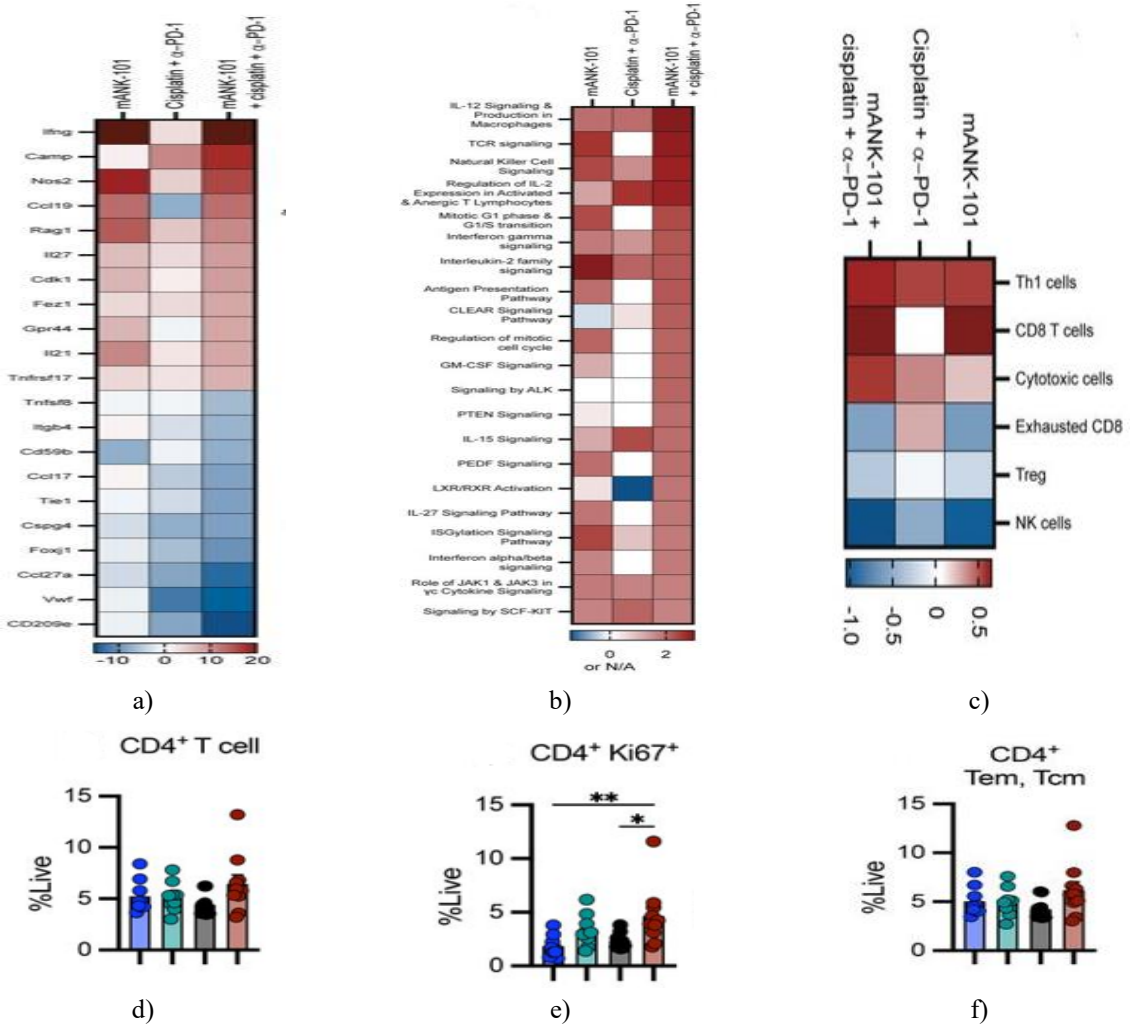

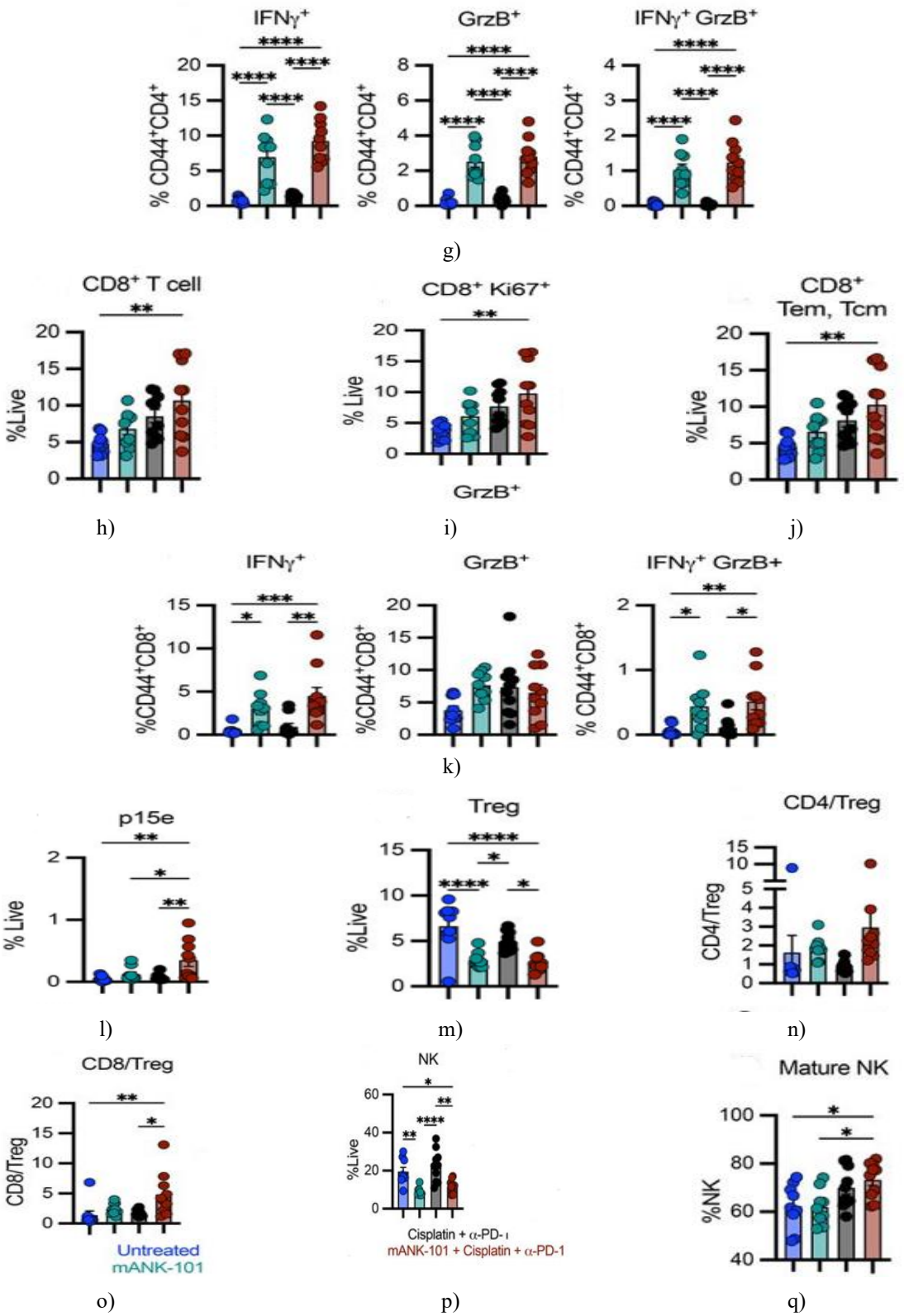

Figure 3. Augmentation of immune effector responses following combined mANK-101, cisplatin, and α-PD-1 therapy.

(a–c) Female C57BL/6 mice (8–12 weeks old; n=5–10 per group) were inoculated subcutaneously with 5×10^6 MOC1 cells on day 0 and treated on day 10 with mANK-101 (5 µg, i.t.), cisplatin (5 mg/kg, i.p.), and α-PD-1 (200 µg, i.p.). On day 15, tumor-derived $CD45^+$ immune cells were isolated and subjected to NanoString Mouse PanCancer IO360 gene expression analysis. Heatmaps display (a) the ten most upregulated and downregulated transcripts in the combination therapy group relative to untreated controls based on fold-change, (b) pathway enrichment results summarized by z-scores, and (c) inferred immune cell composition derived from cell type z-score analysis.

(d–q) Flow cytometric assessment on day 15 quantified (d) total $CD4^+$ T cells, (e) proliferative $Ki67^+$ $CD4^+$ T cells, and (f) memory $CD4^+$ T-cell subsets. Within the $CD44^+CD4^+$ population, functional profiling evaluated the proportions of (g) IFN-γ–producing, granzyme B–expressing, and IFN-γ^+granzyme B^+ cells. Additional analyses measured (h) total $CD8^+$ T cells, (i) cycling $Ki67^+$ $CD8^+$ T cells, and (J) memory $CD8^+$ T-cell subsets. Functional status of $CD44^+CD8^+$ T cells was assessed by (k) IFN-γ and granzyme B expression. Tumor antigen–specific $CD8^+$ T cells were identified using (l) p15e tetramer staining, while (m) $FoxP3^+CD4^+$ regulatory T cells were enumerated. Ratios of (n) $CD4^+$ T cells to Tregs and (o) $CD8^+$ T cells to Tregs were calculated. Innate immune populations were evaluated by measuring (p) $CD49b^+$ NK cells and (q) mature $CD11b^+$ NK cells. Statistical comparisons were conducted using one-way ANOVA with Tukey's post hoc test. Error bars indicate SEM. *p<0.05, **p<0.01, ***p<0.001, ****p<0.0001. Abbreviations: ANOVA, analysis of variance; GrzB, granzyme B; IFN, interferon; i.p., intraperitoneal; i.t., intratumoral; N/A, not applicable; NK, natural killer; PD-1, programmed death 1; Tcm, central memory T cell; Tem, effector memory T cell; Treg, regulatory T cell.

Flow cytometric characterization of tumor-infiltrating lymphocytes revealed no statistically significant differences in the overall abundance of $CD4^+$ effector T cells among treatment groups **(Figure 3d).** Nonetheless, the mANK-101+cisplatin+α-PD-1 regimen significantly increased the proportion of $Ki67^+$ proliferating $CD4^+$ T cells (p=0.0054; **Figure 3e**). The distribution of effector memory (Tem; $CD44^+CD62L^-$) and central memory (Tcm; $CD44^+CD62L^+$) $CD4^+$ T-cell subsets remained largely unchanged across conditions **(Figure 3f).** In contrast, functional analyses demonstrated that $CD4^+$ T cells infiltrating tumors from mice treated with mANK-101 alone or in combination exhibited substantially enhanced IFN-γ and granzyme B production relative to untreated or SOC-treated animals (p<0.0001; **Figure 3g**). Within the $CD8^+$ T-cell compartment, a significant expansion was observed exclusively following mANK-101+cisplatin+α-PD-1 administration (p=0.0021; **Figure 3h)**, including increased frequencies of $Ki67^+$ $CD8^+$ T cells (p=0.0016; **Figure 3i**) and both effector memory and central memory $CD8^+$ subsets (p=0.0020; **Figure 3j**). Further interrogation of $CD44^+CD8^+$ T cells showed elevated IFN-γ expression after mANK-101 monotherapy (p=0.0462) and a more pronounced increase with the triple-combination therapy (p=0.0005). Co-expression of IFN-γ and granzyme B followed a similar pattern (p=0.347 and p=0.007, respectively; **Figure 3k**). Given that MOC1 tumors express the endogenous retroviral antigen p15e [20], the marked enrichment of p15e tetramer–positive $CD8^+$ T cells observed following mANK-101+cisplatin+α-PD-1 treatment **(Figure 3l)** indicates induction of a tumor antigen–specific cytotoxic T-cell response.

Within the tumor microenvironment (TME), the suppressive regulatory T-cell (Treg) compartment was markedly reduced following administration of mANK-101 alone (p<0.0001) or the triple therapy combining mANK-101, cisplatin, and α-PD-1 (p<0.0001; **Figure 3m)**. Despite the drop in Treg numbers, this did not translate into an improved CD4:Treg ratio **(Figure 3n).** In contrast, the concurrent increase in $CD8^+$ T cells observed with the triple combination led to a statistically significant rise in the CD8:Treg ratio (p=0.0071; **Figure 3o).**

Unexpectedly, NK cell frequency in the TME decreased following both mANK-101 and triple therapy treatments **(Figure 3p).** However, the proportion of mature NK cells, defined as $CD11b^+CD27^+$ and $CD11b^+CD27^-$ subsets, increased in the triple therapy group relative to both untreated controls (p=0.0286) and the mANK-101 monotherapy group (p=0.0236; **Figure 3q**).

Triple therapy induces TLS-like immune clusters in MOC1 tumors

Tumor-infiltrating immune cells were analyzed 28 days post-implantation using H&E staining and multiplex immunofluorescence. H&E sections revealed clusters of immune cells localized near the tumor periphery, predominantly in animals treated with mANK-101 alone or in combination with cisplatin and α-PD-1 (**Figure 4a**, right panels). Multiplex staining indicated that these

aggregates were primarily composed of $B220^{+}CD19^{+}$ B cells interspersed with $CD11c^{+}$ dendritic cells and encircled by $CD8^{+}$ T cells, including $CD103^{+}$ tissue-resident memory subsets (**Figure 4a**, middle and right panels). This architecture mirrors tertiary lymphoid structures (TLSs) reported in murine and human tumors [22, 23]. It is hypothesized that p15e-specific $CD8^{+}$ T cells identified by flow cytometry **(Figure 3l)** reside within these TLS-like aggregates; this will require validation using tetramer staining on fresh tissue sections in future studies [24, 25].

Expression of the chemokine CXCL13, known to facilitate the formation and maintenance of ectopic lymphoid structures [26, 27], was detected within the aggregates. Quantitative assessment confirmed an increased prevalence of TLS-like clusters in tumors treated with mANK-101+cisplatin+α-PD-1 **(Figure 4b).** Moreover, the augmented B-cell presence and immune cluster formation coincided with higher circulating anti-MOC1 tumor antibody titers in the triple therapy group **(Figure S4).** These findings support prior evidence that TLSs are associated with improved immunotherapeutic responses [28, 29].

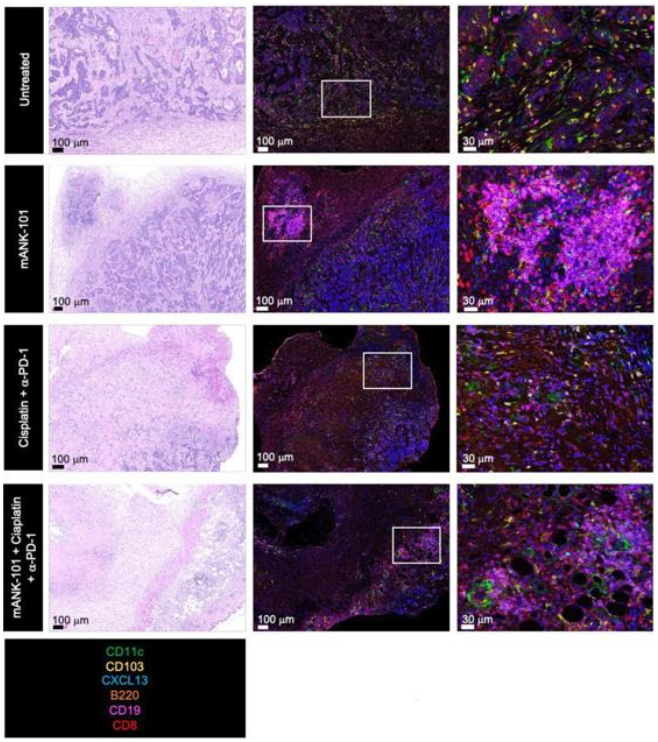

a)

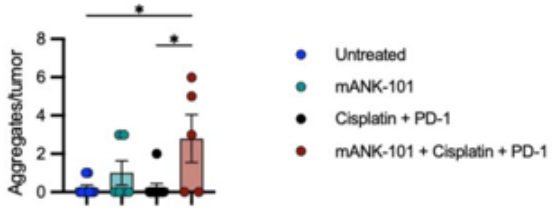

b)

Figure 4. Formation of immune cell clusters in MOC1 tumors after treatment with mANK-101, cisplatin, and α-PD-1

Female C57BL/6 mice (8–12 weeks old; n=8–10/group) were implanted subcutaneously with 5×10^6 MOC1 cells on the right flank on day 0 and treated following the protocol outlined in **Figure 1a**. Tumors were harvested on day 28 and processed for (a) H&E staining (left panels) and multiplex immunofluorescence imaging (middle and right panels). (b) The number of immune aggregates, defined as dense clusters of $B220^+CD19^+$ B cells, $CD11c^+$ dendritic cells, and $CD8^+$ T cells expressing CD103 and CXCL13, was quantified. Statistical comparisons were conducted using one-way ANOVA with Tukey's post hoc analysis. Error bars represent SEM. *p<0.05. ANOVA, analysis of variance; DC, dendritic cell; PD-1, programmed death 1.

Antitumor activity of the triple combination relies on IFN-γ

To determine the immune components required for the efficacy of mANK-101+cisplatin+α-PD-1, targeted depletion studies were performed. Simultaneous removal of $CD4^+$ T cells, $CD8^+$ T cells, and NK cells strongly impaired tumor suppression (p<0.0001; **Figure 5a**) and reduced survival (p<0.0001; **figure 5b**). Blocking IFN-γ also significantly decreased tumor growth control (p<0.0001; **Figure 5c**) and diminished the survival benefit of the combination therapy (p=0.0001; **Figure 5d**). These results indicate that both effector lymphocytes and IFN-γ are essential contributors to the antitumor response, although no single component fully accounted for the therapy's effect, highlighting its multifaceted nature.

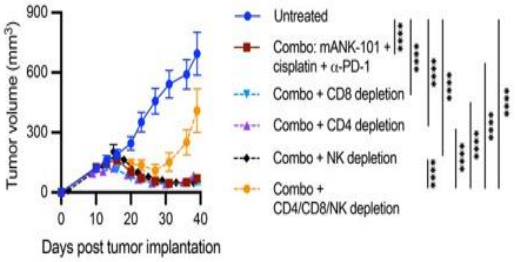

a)

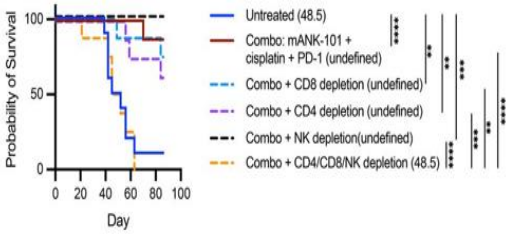

b)

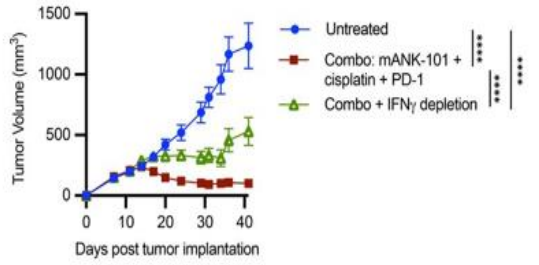

c)

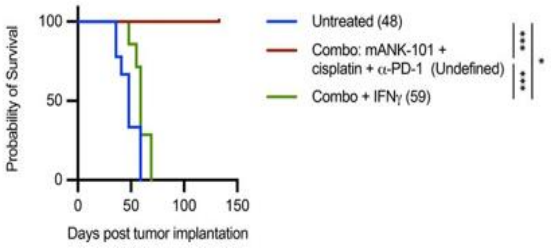

d)

Figure 5. Dependence of mANK-101+cisplatin+α-PD-1 therapy on effector lymphocytes and IFN-γ

Female C57BL/6 mice (8–12 weeks old; n=8–10/group) received 5×10^6 MOC1 cells on day 0 and were treated as described in **Figure 1a**. (a–b) Antibodies for CD4 (100 µg, i.p.), CD8 (100 µg, i.p.), and NK1.1 (100 µg, i.p.) were administered on days 6, 7, and 8, and weekly thereafter. Tumor growth and survival were monitored; numbers in parentheses indicate median overall survival (mOS). (c–d) IFN-γ neutralizing antibody (100 µg, i.p.) was given 2 days before, on the day of, and 2 days after treatment, then three times per week. Tumor growth over time and survival were tracked. Tumor growth comparisons were performed using two-way ANOVA with Tukey's post hoc test; survival was analyzed via the Mantel-Cox test. Error bars indicate SEM. *p<0.05, **p<0.01, ***p<0.001, ****p<0.0001. ANOVA, analysis of variance; IFN, interferon; i.p., intraperitoneal; mOS, median overall survival; PD-1, programmed death 1.

Shift of TAMs from M2 to M1 in the TME after therapy

Most tumor-associated macrophages (TAMs) are derived from circulating monocytes, with MCP-1 being a key chemokine for recruitment [30, 31]. In mice receiving mANK-101+cisplatin+α-PD-1, MCP-1 concentrations were significantly elevated in serum (p=0.003) and tumor tissue (p=0.0007; **Figure 6a**). mANK-101 monotherapy also led to a substantial increase in intratumoral MCP-1 (p<0.0001; **Figure 6a**). Total macrophage numbers in the

TME remained unchanged **(Figure 6b)**; however, both mANK-101 alone and the triple therapy increased pro-inflammatory M1 macrophages ($CD38^{+}CD206^{-}$; **Figure 6c)** while reducing pro-tumor M2 macrophages ($CD38^{-}CD206^{+}$; **Figure 6d**; $p<0.0001$ vs control). Consequently, the M1/M2 ratio improved significantly in mANK-101 ($p=0.0325$) and triple therapy-treated groups ($p=0.0013$; **Figure 6e**).

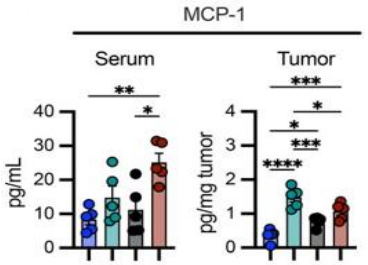

a)

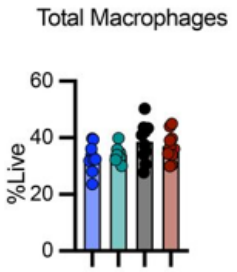

b)

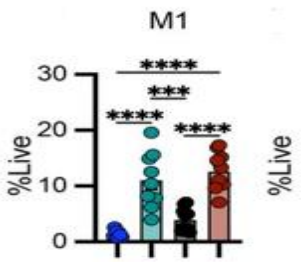

c)

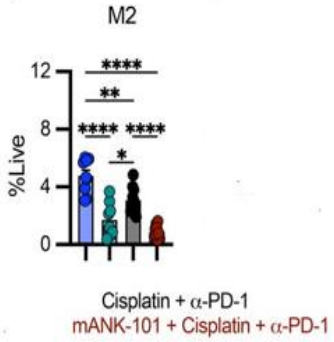

d)

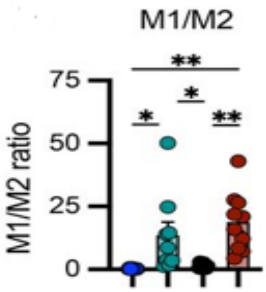

e)

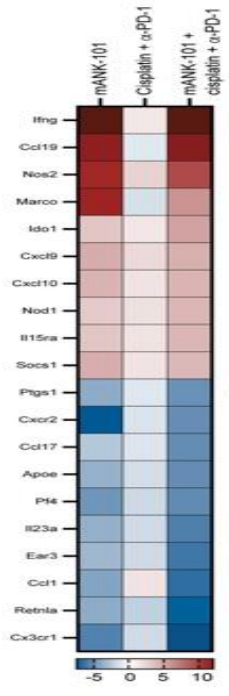

f)

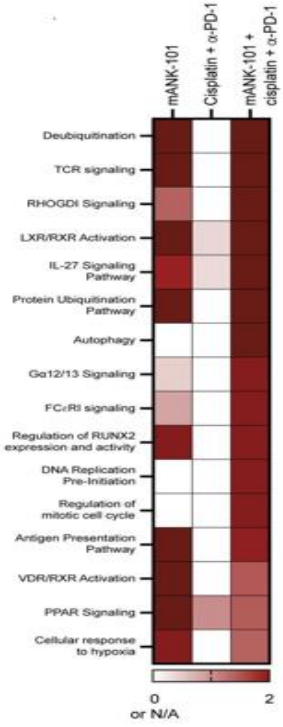

g)

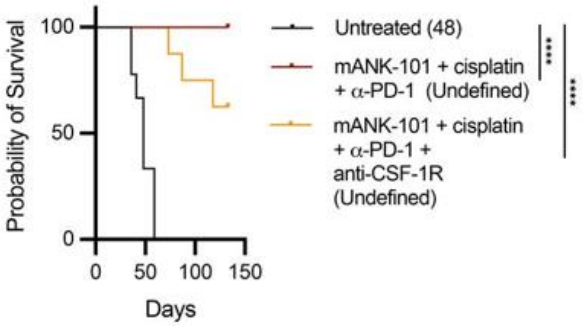

h)

Figure 6. Triple treatment with mANK-101, cisplatin, and α-PD-1 drives M2-to-M1 macrophage polarization in the tumor microenvironment

Female C57BL/6 mice (8–12 weeks old; n=8–10/group) were injected with 5×10^6 MOC1 cells in the right flank on day 0. Treatments included mANK-101 (5 µg, intratumoral), cisplatin (5 mg/kg, intraperitoneal), and α-PD-1 (200 µg, intraperitoneal). On day 15, serum and tumor samples were collected for the measurement of (a) MCP-1. Flow cytometry of tumor tissue was used to evaluate (b) total macrophages ($CD11b^+F4/80^+$), (c) M1 macrophages ($CD11b^+F4/80^+CD38^+CD206^-$), (d) M2 macrophages ($CD11b^+F4/80^+CD38^-CD206^+$), and (e) the M1/M2 ratio.

(f) RNA sequencing of $CD45^+$ tumor-infiltrating cells was conducted using the NanoString Myeloid Innate Immunity Panel. Heatmaps display (f) the 10 most upregulated and downregulated genes in the combination-treated group versus untreated controls, and (g) pathway enrichment z-scores.

(h) A separate cohort received the same treatment as in **Figure 1a**, with CSFR1-neutralizing antibody (100 µg, intraperitoneal) administered 2 days before treatment, on the treatment day, and 2 days afterward, repeated three times weekly. Survival was tracked. Statistical analyses: one-way ANOVA with Tukey's post hoc test for group comparisons, Mantel-Cox test for survival. Error bars: SEM. *$p<0.05$. ANOVA, analysis of variance; i.p., intraperitoneal; i.t., intratumoral; MCP, monocyte chemoattractant protein; M1, type 1 macrophage; M2, type 2 macrophage; PD-1, programmed death 1.

RNA data showed that genes linked to M1 macrophage activity, such as **Ifng, Cxcl9, and Cxcl10**, were upregulated in both mANK-101 alone and the triple therapy group [32] **(Figure 6f).** Associated pathways, including antigen presentation and regulatory mechanisms like LXR/RXR signaling and ubiquitination/deubiquitination, were enhanced **(Figure 6g).** Triple therapy without macrophage depletion achieved 100% survival, whereas combining therapy with macrophage depletion reduced survival to 62.5% (**Figure 6h**). Despite not reaching significance ($p=0.0628$), this trend indicates a substantial contribution of macrophages to therapeutic outcomes.

Abscopal effects of mANK-101+cisplatin+α-PD-1

Previous studies indicated that intratumoral mANK-101 can induce regression of untreated distant tumors in Ag410A, B16F10, and MC38 models [15, 16]. To test this effect in combination therapy, mice with bilateral MOC1 tumors were injected with mANK-101 in the right tumor, alongside systemic cisplatin and α-PD-1. In this model, cisplatin+α-PD-1 suppressed both tumors ($p<0.0001$; **Figure 7a).**

In the injected tumor, mANK-101 alone or with cisplatin+α-PD-1 showed enhanced regression compared to untreated controls ($p<0.0001$ for both) and SOC ($p=0.0041$ and $p=0.0011$, respectively), but these two regimens did not differ significantly from each other ($p=0.9834$).

For the contralateral, uninjected tumor, mANK-101 alone produced effects similar to cisplatin+α-PD-1 ($p=0.8324$). However, the triple combination significantly reduced tumor size compared with mANK-101 monotherapy ($p=0.0089$) and SOC ($p=0.0006$), indicating a clear systemic, abscopal antitumor response.

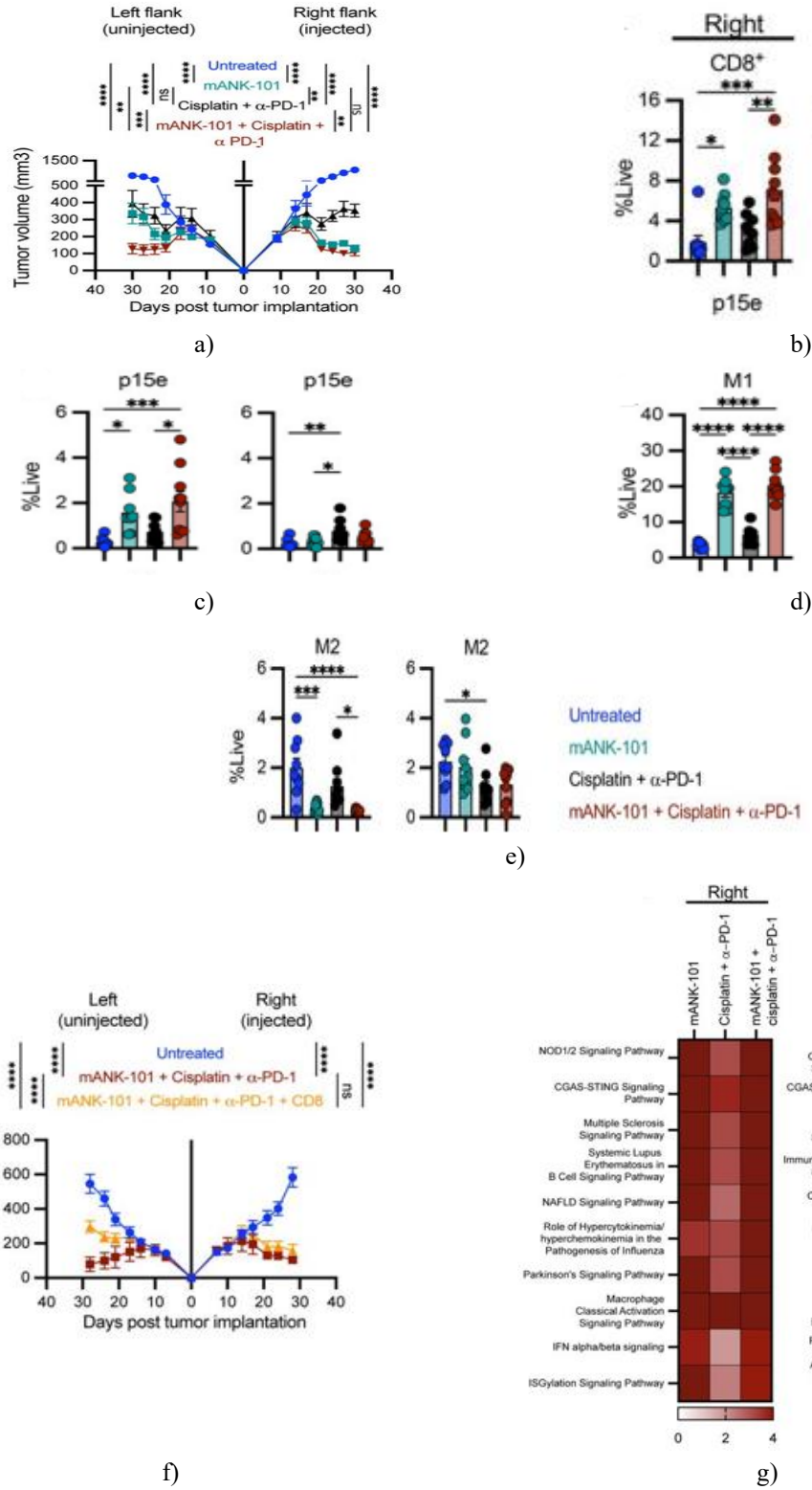

Figure 7. mANK-101+cisplatin+α-PD-1 combination induces systemic antitumor effects in MOC1 tumors

Female C57BL/6 mice (8–12 weeks old; n=8/group) were implanted bilaterally with 5×10^6 MOC1 cells in the right and left flanks on day 0. Treatment followed the schematic in **Figure 1a**, with only the right tumor

receiving an intratumoral injection of 5 µg mANK-101; the left tumor remained untreated.

(a) Tumor sizes were tracked for both flanks. On day 15, tumors were collected for flow cytometry to evaluate: (b) $CD8^+$ T cells, (c) p15e tetramer$^+$ $CD8^+$ T cells, (D) M1 macrophages ($CD11b^+F4/80^+CD38^+CD206^-$), and (e) M2 macrophages ($CD11b^+F4/80^+CD38^-CD206^+$).

(f) In a separate cohort (n=9–10/group), mice underwent combination therapy alongside $CD8^+$ T-cell depletion (100 µg, i.p.) on days 6–8, then weekly. Tumor growth on both flanks was monitored, and $CD45^+$ tumor-infiltrating cells were isolated on day 15 for RNA profiling using the NanoString Mouse PanCancer IO360 panel. (g) Heatmaps displaying enriched pathways in right (injected) and left (distal) tumors were generated. Statistical tests: tumor growth via one- or two-way ANOVA with Tukey's post hoc test; group comparisons by one-way ANOVA with Tukey correction. Error bars indicate SEM. *p<0.05, **p<0.01, ***p<0.001, ****p<0.0001. ANOVA, analysis of variance; IFN, interferon; i.p., intraperitoneal; M1, type 1 macrophage; M2, type 2 macrophage; PD-1, programmed death 1.

Flow cytometry demonstrated that mANK-101 monotherapy and triple therapy increased $CD8^+$ T-cell infiltration **(Figure 7b),** expanded p15e tetramer$^+$ $CD8^+$ T cells **(Figure 7c),** enhanced M1 macrophage numbers **(Figure 7d),** and decreased M2 macrophage frequency **(Figure 7e)** in the injected tumors five days post-treatment. In the distant, uninjected tumors, mANK-101 alone had negligible effects. However, the combination therapy increased $CD8^+$ T-cell infiltration (p=0.0319; **Figure 7b)** and M1 macrophages (p=0.0085; **Figure 7d)** in distal tumors, although not to the levels observed in injected tumors. Cisplatin+α-PD-1 alone did not significantly alter immune populations in either tumor.

To investigate $CD8^+$ T-cell involvement in the systemic (abscopal) effect, mice receiving combination therapy underwent $CD8^+$ T-cell depletion. In injected tumors, $CD8^+$ T cells were not critical for tumor suppression **(Figure 7f).** By contrast, depletion in distal tumors substantially reduced the antitumor effect (p<0.0001; **Figure 7f),** indicating that $CD8^+$ T cells are key mediators of the abscopal response.

RNA pathway analysis revealed that combination therapy activated immune-related signaling in both injected and distal tumors **(Figure 7g).** Innate immune pathways, including NOD1/2, CGAS/STING, and classical macrophage activation, were upregulated in both tumor sites. In injected tumors, pathways induced by combination therapy overlapped with those stimulated by mANK-101 alone. In distal tumors, pathway activation differed: while IL-12 and IL-27 signaling were moderately elevated in both monotherapy and combination therapy, only the triple therapy promoted the three innate immune pathways; these were downregulated in distal tumors of the mANK-101 monotherapy group.

The KEYNOTE-048 trial established that patients with metastatic or unresectable recurrent HNSCC experienced improved overall survival when treated with pembrolizumab, either alone or alongside chemotherapy [4, 5]. Following these findings, pembrolizumab monotherapy is now endorsed as the primary treatment for PD-L1-positive HNSCC, whereas the combination of pembrolizumab with cisplatin or carboplatin plus fluorouracil is recommended irrespective of PD-L1 expression. While these strategies extended median overall survival compared with cetuximab plus chemotherapy, they did not significantly impact progression-free survival or objective response rates. Further subgroup analyses revealed that the benefit of pembrolizumab, with or without chemotherapy, was closely linked to PD-L1 levels. For patients with a PD-L1 CPS below 1, pembrolizumab-based regimens did not outperform cetuximab plus chemotherapy [33]. Preclinical studies indicate that mANK-101 can elevate PD-L1 expression within tumors [16], supporting the rationale for integrating intratumoral IL-12 with standard SOC therapies.

Our study provides preclinical data suggesting that ANK-101 could complement SOC chemotherapy and pembrolizumab for R/M HNSCC, particularly in PD-L1 CPS<1 settings. In the MOC1 tumor model, combining mANK-101 with cisplatin and α-PD-1 enhanced tumor regression and increased the proportion of tumor-free mice relative to mANK-101 alone or SOC cisplatin+α-PD-1. The results also imply that evaluating ANK-101 with pembrolizumab alone may be worthwhile, as the doublet demonstrated measurable antitumor activity in this model. Although the current experiments utilized HPV-negative tumors, the approach could be extended to HPV-positive patients, since current clinical guidelines for SOC immunotherapy in R/M HNSCC do not differentiate by HPV status [34]. Future trials should assess whether HPV status influences ANK-101 response rates in combination with SOC.

These findings corroborate prior work showing that anchored mANK-101 elicits robust antitumor responses

across various syngeneic models, whether as monotherapy or combined with immune checkpoint inhibitors [15, 16]. The antitumor effect is associated with prolonged tumor retention of IL-12, which increases the therapeutic window while minimizing systemic toxicity. In this study, IL-12 was further maintained in tumors for longer periods when combined with cisplatin and α-PD-1 **(Figure 1g).** Serum IL-12 showed transient elevations before returning to baseline **(Figure 1g);** whether this reflects a self-amplifying feedback loop or cytokine leakage remains unclear. Notably, no adverse effects were observed, with body weight remaining stable **(Figure 2e).**

The majority of patients with HNSCC present with locoregional disease, and over two-thirds of relapsed patients show locoregional recurrence [35]. Like cutaneous tumors, newly diagnosed or recurrent mucosal tumors are accessible to intratumoral injection [14]. Although local inflammatory reactions are possible, the anatomical accessibility supports early-phase clinical testing of ANK-101 in combination with SOC.

Previous studies demonstrated that mANK-101 enhances T-cell infiltration and functional activity within tumors [15, 16]. Phase I trials in canines with advanced oral melanoma (cANK-101) also revealed increased intratumoral immune infiltration and elevated circulating IFN-γ [36]. Consistent with these findings, the potent antitumor effect of the mANK-101+cisplatin+α-PD-1 combination in the MOC1 model correlated with heightened $CD8^+$ T-cell infiltration and activity **(Figure 3)** and increased tumoral IFN-γ **(Figure 1h).** Interestingly, $CD8^+$ T-cell depletion alone did not compromise therapy efficacy; a decrease in antitumor benefit occurred only when $CD4^+$ T cells, $CD8^+$ T cells, and NK cells were concurrently depleted, indicating a compensatory or cooperative interaction among lymphocyte subsets. IFN-γ, produced by multiple activated immune cells and known for its role in tumor regression [37], emerged as a critical mediator of the antitumor response induced by mANK-101+cisplatin+α-PD-1, as supported by RNA, flow cytometry, and depletion studies.

Furthermore, the combination therapy generated a durable immune memory, protecting mice against both tumor rechallenge and growth of distant tumors **(Figures 1e and 7a).** Depletion studies revealed that $CD8^+$ T cells are crucial for the abscopal effect, although p15e-specific T cells were not detected in distal tumors at the time point analyzed **(Figure 7).** It is possible that these T cells infiltrated later, or that other T-cell populations recognizing neoantigens contributed more prominently in the distal site. In any case, mANK-101's capacity to enhance antigen presentation [15], together with PD-1–driven T-cell activation, likely worked synergistically to improve overall antitumor efficacy. Cisplatin may further sensitize tumor cells to immune-mediated killing [38, 39], which could explain the stronger regression observed in distal tumors in the triple therapy compared with mANK-101 alone.

The TME of HNSCC is densely populated with TAMs, predominantly of the M2 phenotype, which promote immunosuppression and tumor progression and correlate with poor patient outcomes [40, 41]. Thus, the observed repolarization of TAMs from M2 toward the antitumorigenic M1 phenotype by mANK-101+cisplatin+α-PD-1 is a key therapeutic feature. MCP-1, a chemokine driving monocyte recruitment [30, 31], increased following combination treatment, yet total macrophage numbers remained unchanged **(Figures 6a and 6b)**. The role of MCP-1 in guiding M1 versus M2 differentiation is context-dependent, influenced by cytokine environment, tumor metabolism, and other local factors [31, 42]. IFN-γ is a critical mediator of M1 polarization and maintenance [43, 44] and also upregulates CXCL9 and CXCL10 **(Figure 6f).** CXCL9/10 derived from macrophages are required for effective immune checkpoint therapy [45] and likely contribute to the enhanced antitumor activity seen with mANK-101 plus SOC in MOC1 tumors, as previously reported in other models [16].

Another important mechanism of the mANK-101+cisplatin+α-PD-1 response is the induction of TLS-like immune aggregates. TLSs, defined by B cell–rich follicles with adjacent mature DCs and T-cell zones, are associated with effective antitumor immunity [22, 23, 28, 29]. Within these structures, DCs present tumor antigens to T cells, promoting local priming, T-cell activation, and memory formation [22, 23]. Previous studies indicate that B–T cell interactions in TLSs contribute to abscopal effects in models of intratumoral IL-12 plus CpG [46]. While TLS biology in cancer remains incompletely understood, these aggregates likely enhance the speed and efficiency of local immune responses and provide a niche supporting effector cells [23]. TLS presence correlates with better survival in several cancer types [47, 48] and improved responses to immune checkpoint blockade [28, 29]. In HNSCC, TLS signatures are more prevalent in HPV^+ patients than in HPV^- cases [49, 50].

In this study, mANK-101 alone induced TLS-like structures in HPV⁻ MOC1 tumors, and combination therapy further augmented their formation **(Figure 4).** Future studies should confirm these structures as bona fide TLSs by detecting germinal center B cells, follicular DCs, and high endothelial venules [50, 51]. These observations are consistent with prior clinical data showing intratumoral IL-12 promotes peritumoral B-cell infiltration in HNSCC [52]. The mechanisms by which mANK-101, cisplatin, and α-PD-1 drive TLS formation, and potential differences between HPV⁺ and HPV⁻ tumors, remain to be explored. Additionally, the role of humoral immunity in mediating the observed antitumor effect requires further investigation. Prior work has linked intratumoral IL-12 plus CpG with systemic antitumor antibodies [46]. In the current study, increased B-cell infiltration **(Figure 4)** and activation of the systemic lupus erythematosus B-cell pathway [53] coincided with anti-MOC1 antibody production in mice receiving the triple therapy. The specificity and contribution of these antibodies to the antitumor response remain to be elucidated.

The ongoing ANCHOR trial, the first-in-human evaluation of the human analog of mANK-101, will provide data on safety, tolerability, pharmacokinetics, and pharmacodynamics, guiding future combination strategies with alum-tethered IL-12. In this preclinical study, mANK-101+cisplatin+α-PD-1 therapy enhanced tumor control, increased effector cell infiltration and function, promoted TLS-like aggregates, and shifted TAMs toward an M1 phenotype. Collectively, these findings support combining alum-tethered IL-12 with standard HNSCC therapy and indicate potential efficacy even in patients with low PD-L1 expression.

Acknowledgments: The authors thank Debra Weingarten for her editorial assistance in the preparation of this manuscript.

Conflict of Interest: None

Financial Support: This work was funded by the Intramural Research Program of the Center for Cancer Research, National Cancer Institute, National Institutes of Health (ZIA BC 010944), as well as via a Cooperative Research and Development Agreement between the National Cancer Institute and Ankyra Therapeutics (Cambridge, Massachusetts, USA).

Ethics Statement: All animal experimental studies were performed under the approval of the NIH Intramural Animal Care and Use Committee. All mice were housed and maintained in accordance with the Association for Assessment and Accreditation of Laboratory Animal Care (AAALAC) guidelines: NIH AALAC approval: CIO-2.

References

1. Barsouk A, Aluru JS, Rawla P, et al. Epidemiology, Risk Factors, and Prevention of Head and Neck Squamous Cell Carcinoma. Med Sci (Basel) 2023;11 doi: 10.3390/medsci11020042
2. Solomon B, Young RJ, Rischin D. Head and neck squamous cell carcinoma: Genomics and emerging biomarkers for immunomodulatory cancer treatments. Semin Cancer Biol. 2018;52:228–40. doi: 10.1016/j.semcancer.2018.01.008
3. Johnson DE, Burtness B, Leemans CR, et al. Head and neck squamous cell carcinoma. Nat Rev Dis Primers. 2020;6:92. doi: 10.1038/s41572-020-00224-3
4. Burtness B, Harrington KJ, Greil R, et al. Pembrolizumab alone or with chemotherapy versus cetuximab with chemotherapy for recurrent or metastatic squamous cell carcinoma of the head and neck (KEYNOTE-048): a randomised, open-label, phase 3 study. Lancet. 2019;394:1915–28. doi: 10.1016/S0140-6736(19)32591-7
5. Harrington KJ, Burtness B, Greil R, et al. Pembrolizumab With or Without Chemotherapy in Recurrent or Metastatic Head and Neck Squamous Cell Carcinoma: Updated Results of the Phase III KEYNOTE-048 Study. J Clin Oncol. 2023;41:790–802. doi: 10.1200/JCO.21.02508
6. Lasek W, Zagożdżon R, Jakobisiak M. Interleukin 12: still a promising candidate for tumor immunotherapy? Cancer Immunol Immunother. 2014;63:419–35. doi: 10.1007/s00262-014-1523-1
7. Jia Z, Ragoonanan D, Mahadeo KM, et al. IL12 immune therapy clinical trial review: Novel strategies for avoiding CRS-associated cytokines. Front Immunol. 2022;13:952231. doi: 10.3389/fimmu.2022.952231
8. Cirella A, Luri-Rey C, Di Trani CA, et al. Novel strategies exploiting interleukin-12 in cancer immunotherapy. Pharmacol Ther. 2022;239:108189. doi: 10.1016/j.pharmthera.2022.108189

9. Thaker PH, Brady WE, Lankes HA, et al. A phase I trial of intraperitoneal GEN-1, an IL-12 plasmid formulated with PEG-PEI-cholesterol lipopolymer, administered with pegylated liposomal doxorubicin in patients with recurrent or persistent epithelial ovarian, fallopian tube or primary peritoneal cancers: An NRG Oncology/Gynecologic Oncology Group study. Gynecol Oncol. 2017;147:283–90. doi: 10.1016/j.ygyno.2017.08.001
10. Strauss J, Heery CR, Kim JW, et al. First-in-Human Phase I Trial of a Tumor-Targeted Cytokine (NHS-IL12) in Subjects with Metastatic Solid Tumors. Clin Cancer Res. 2019;25:99–109. doi: 10.1158/1078-0432.CCR-18-1512
11. Gatti-Mays ME, Tschernia NP, Strauss J, et al. A Phase I Single-Arm Study of Biweekly NHS-IL12 in Patients With Metastatic Solid Tumors. Oncologist. 2023;28:364–e217. doi: 10.1093/oncolo/oyac244
12. .Castañón E, Zamarin D, Carneiro BA, et al. Abstract CT004: Intratumoral (IT) MEDI1191 + durvalumab (D): Update on the first-in-human study in advanced solid tumors. Cancer Res. 2023;83:CT004. doi: 10.1158/1538-7445.AM2023-CT004
13. Bechter O, Loquai C, Champiat S, et al. Abstract LB198: A first-in-human, open-label, multicenter study of intratumoral SAR441000 (mixture of cytokine encoding mRNAs), as monotherapy and in combination with cemiplimab in patients with advanced solid tumors. Cancer Res. 2023;83:LB198. doi: 10.1158/1538-7445.AM2023-LB198
14. Jiménez-Labaig P, Rullan A, Braña I, et al. Intratumoral therapies in head and neck squamous cell carcinoma: A systematic review and future perspectives. Cancer Treat Rev. 2024;127:102746. doi: 10.1016/j.ctrv.2024.102746
15. Agarwal Y, Milling LE, Chang JYH, et al. Intratumourally injected alum-tethered cytokines elicit potent and safer local and systemic anticancer immunity. Nat Biomed Eng. 2022;6:129–43. doi: 10.1038/s41551-021-00831-9
16. Battula S, Papastoitsis G, Kaufman HL, et al. Intratumoral aluminum hydroxide-anchored IL-12 drives potent antitumor activity by remodeling the tumor microenvironment. JCI Insight. 2023;8:e168224. doi: 10.1172/jci.insight.168224.
17. Judd NP, Allen CT, Winkler AE, et al. Comparative analysis of tumor-infiltrating lymphocytes in a syngeneic mouse model of oral cancer. Otolaryngol Head Neck Surg. 2012;147:493–500. doi: 10.1177/0194599812442037
18. Kilkenny C, Browne WJ, Cuthill IC, et al. Improving bioscience research reporting: the ARRIVE guidelines for reporting animal research. PLoS Biol. 2010;8:e1000412. doi: 10.1371/journal.pbio.1000412
19. Hanemaaijer SH, Kok IC, Fehrmann RSN, et al. Comparison of Carboplatin With 5-Fluorouracil vs. Cisplatin as Concomitant Chemoradiotherapy for Locally Advanced Head and Neck Squamous Cell Carcinoma. Front Oncol. 2020;10:761. doi: 10.3389/fonc.2020.00761.
20. Moore EC, Cash HA, Caruso AM, et al. Enhanced Tumor Control with Combination mTOR and PD-L1 Inhibition in Syngeneic Oral Cavity Cancers. Cancer Immunol Res. 2016;4:611–20. doi: 10.1158/2326-6066.CIR-15-0252
21. Duan Q, Zhang H, Zheng J. Turning Cold into Hot: Firing up the Tumor Microenvironment. Trends Cancer. 2020;6:605–18. doi: 10.1016/j.trecan.2020.02.022
22. Sautès-Fridman C, Petitprez F, Calderaro J, et al. Tertiary lymphoid structures in the era of cancer immunotherapy. Nat Rev Cancer. 2019;19:307–25. doi: 10.1038/s41568-019-0144-6
23. Schumacher TN, Thommen DS. Tertiary lymphoid structures in cancer. Science. 2022;375:eabf9419. doi: 10.1126/science.abf9419
24. Li S, Mwakalundwa G, Skinner PJ. In Situ MHC-tetramer Staining and Quantitative Analysis to Determine the Location, Abundance, and Phenotype of Antigen-specific CD8 T Cells in Tissues. J Vis Exp. 2017:56130. doi: 10.3791/56130
25. Abdelaal HM, Cartwright EK, Skinner PJ. Detection of Antigen-Specific T Cells Using In Situ MHC Tetramer Staining. Int J Mol Sci. 2019;20:5165. doi: 10.3390/ijms20205165
26. Workel HH, Lubbers JM, Arnold R, et al. A Transcriptionally Distinct CXCL13+CD103+CD8+ T-cell Population Is Associated with B-cell Recruitment and Neoantigen Load in Human Cancer. Cancer Immunol Res. 2019;7:784–96. doi: 10.1158/2326-6066.CIR-18-0517
27. Li H, Ding J-Y, Zhang M-J, et al. Tertiary lymphoid structures and cytokines interconnections: The implication in cancer immunotherapy. Cancer Lett. 2023;568:216293. doi: 10.1016/j.canlet.2023.216293

28. Cabrita R, Lauss M, Sanna A, et al. Tertiary lymphoid structures improve immunotherapy and survival in melanoma. Nature New Biol. 2020;577:561–5. doi: 10.1038/s41586-019-1914-8
29. Helmink BA, Reddy SM, Gao J, et al. B cells and tertiary lymphoid structures promote immunotherapy response. Nature New Biol. 2020;577:549–55. doi: 10.1038/s41586-019-1922-8
30. Richards DM, Hettinger J, Feuerer M. Monocytes and macrophages in cancer: development and functions. Cancer Microenviron. 2013;6:179–91. doi: 10.1007/s12307-012-0123-x.
31. DeNardo DG, Ruffell B. Macrophages as regulators of tumour immunity and immunotherapy. Nat Rev Immunol. 2019;19:369–82. doi: 10.1038/s41577-019-0127-6
32. Murray PJ, Allen JE, Biswas SK, et al. Macrophage activation and polarization: nomenclature and experimental guidelines. Immunity. 2014;41:14–20. doi: 10.1016/j.immuni.2014.06.008
33. Burtness B, Rischin D, Greil R, et al. Pembrolizumab Alone or With Chemotherapy for Recurrent/Metastatic Head and Neck Squamous Cell Carcinoma in KEYNOTE-048: Subgroup Analysis by Programmed Death Ligand-1 Combined Positive Score. JCO. 2022;40:2321–32. doi: 10.1200/JCO.21.02198
34. Cohen EEW, Bell RB, Bifulco CB, et al. The Society for Immunotherapy of Cancer consensus statement on immunotherapy for the treatment of squamous cell carcinoma of the head and neck (HNSCC) j immunotherapy cancer. 2019;7:184. doi: 10.1186/s40425-019-0662-5
35. Haring CT, Kana LA, Dermody SM, et al. Patterns of recurrence in head and neck squamous cell carcinoma to inform personalized surveillance protocols. Cancer. 2023;129:2817–27. doi: 10.1002/cncr.34823
36. Barbosa MMP, Lopez AJ, Uyehara R, et al. Abstract 6347: Preliminary results of an exploratory phase I clinical trial of anchored canine interleukin-12 (cANK-101) in dogs with advanced oral malignant melanoma. Cancer Res. 2023;83:6347. doi: 10.1158/1538-7445.AM2023-6347
37. Jorgovanovic D, Song M, Wang L, et al. Roles of IFN-γ in tumor progression and regression: a review. Biomark Res. 2020;8:49. doi: 10.1186/s40364-020-00228-x
38. Fabian KP, Wolfson B, Hodge JW. From Immunogenic Cell Death to Immunogenic Modulation: Select Chemotherapy Regimens Induce a Spectrum of Immune-Enhancing Activities in the Tumor Microenvironment. Front Oncol. 2021;11:728018. doi: 10.3389/fonc.2021.728018
39. Fabian KP, Kowalczyk JT, Reynolds ST, et al. Dying of Stress: Chemotherapy, Radiotherapy, and Small-Molecule Inhibitors in Immunogenic Cell Death and Immunogenic Modulation. Cells. 2022;11:3826. doi: 10.3390/cells11233826
40. Curry JM, Sprandio J, Cognetti D, et al. Tumor microenvironment in head and neck squamous cell carcinoma. Semin Oncol. 2014;41:217–34. doi: 10.1053/j.seminoncol.2014.03.003
41. Kumar AT, Knops A, Swendseid B, et al. Prognostic Significance of Tumor-Associated Macrophage Content in Head and Neck Squamous Cell Carcinoma: A Meta-Analysis. Front Oncol. 2019;9:656. doi: 10.3389/fonc.2019.00656
42. Gschwandtner M, Derler R, Midwood KS. More Than Just Attractive: How CCL2 Influences Myeloid Cell Behavior Beyond Chemotaxis. Front Immunol. 2019;10:2759. doi: 10.3389/fimmu.2019.02759
43. Chen S, Saeed AFUH, Liu Q, et al. Macrophages in immunoregulation and therapeutics. Signal Transduct Target Ther. 2023;8:207. doi: 10.1038/s41392-023-01452-1
44. Mosser DM, Hamidzadeh K, Goncalves R. Macrophages and the maintenance of homeostasis. Cell Mol Immunol . 2021;18:579–87. doi: 10.1038/s41423-020-00541-3
45. House IG, Savas P, Lai J, et al. Macrophage-Derived CXCL9 and CXCL10 Are Required for Antitumor Immune Responses Following Immune Checkpoint Blockade. Clin Cancer Res. 2020;26:487–504. doi: 10.1158/1078-0432.CCR-19-1868
46. Sagiv-Barfi I, Czerwinski DK, Shree T, et al. Intratumoral immunotherapy relies on B and T cell collaboration. Sci Immunol. 2022;7:eabn5859. doi: 10.1126/sciimmunol.abn5859
47. Messina JL, Fenstermacher DA, Eschrich S, et al. 12-Chemokine gene signature identifies lymph node-like structures in melanoma: potential for patient selection for immunotherapy. Sci Rep. 2012;2:765. doi: 10.1038/srep00765
48. Coppola D, Nebozhyn M, Khalil F, et al. Unique Ectopic Lymph Node-Like Structures Present in

Human Primary Colorectal Carcinoma Are Identified by Immune Gene Array Profiling. Am J Pathol. 2011;179:37–45. doi: 10.1016/j.ajpath.2011.03.007

49. .Wood O, Woo J, Seumois G, et al. Gene expression analysis of TIL rich HPV-driven head and neck tumors reveals a distinct B-cell signature when compared to HPV independent tumors. Oncotarget. 2016;7:56781–97. doi: 10.18632/oncotarget.10788
50. Ruffin AT, Cillo AR, Tabib T, et al. B cell signatures and tertiary lymphoid structures contribute to outcome in head and neck squamous cell carcinoma. Nat Commun. 2021;12:3349. doi: 10.1038/s41467-021-23355-x
51. Wirsing AM, Ervik IK, Seppola M, et al. Presence of high-endothelial venules correlates with a favorable immune microenvironment in oral squamous cell carcinoma. Mod Pathol. 2018;31:910–22. doi: 10.1038/s41379-018-0019-5
52. van Herpen CML, van der Laak JAWM, de Vries IJM, et al. Intratumoral recombinant human interleukin-12 administration in head and neck squamous cell carcinoma patients modifies locoregional lymph node architecture and induces natural killer cell infiltration in the primary tumor. Clin Cancer Res. 2005;11:1899–909. doi: 10.1158/1078-0432.CCR-04-1524
53. Nashi E, Wang Y, Diamond B. The role of B cells in lupus pathogenesis. Int J Biochem Cell Biol. 2010;42:543–50. doi: 10.1016/j.biocel.2009.10.011